RSC Advances

PAPER

View Article Online
View Journal | View Issue

Cite this: *RSC Adv.*, 2024, **14**, 1794

A floating photocatalytic fabric integrated with a AgI/UiO-66-NH_2 heterojunction as a facile strategy for wastewater treatment†

Jaeseon Yoo,[a] Jinwook Lee[a] and Jooyoun Kim *[ab]

With an increased need of wastewater treatment, application of photocatalysts has drawn growing research attention as an advanced water remediation strategy. Herein, a floating photocatalytic fabric in a woven construction was developed for removal of Rhodamine B (RhB) in water. For an efficient photocatalytic reaction, AgI nanoparticles were grown on the surface of UiO-66-NH_2 crystals in a layered structure, forming a heterojunction system on a cotton yarn, and this was woven with polypropylene yarn. The floating photocatalyst demonstrated the maximized light utilization and adequate contact with contaminated water. Through the heterojunction system, the electrons and holes were effectively separated to generate reactive chemical species, and this eventually led to an enhanced photocatalytic performance of AgI/UiO@fabric reaching 98% removal efficiency after 2 hours of irradiation. Photodegradation of RhB occurred mainly by superoxide radicals and holes, which were responsible for de-ethylation and decomposition of an aromatic ring, respectively. The kinetics of the photocatalytic reaction suggested that circulation of solution by stirring affected the photocatalytic removal rate. The recycle test demonstrated the potential long-term applicability of the developed material with structural integrity and catalytic stability. This study highlights the proof-of-concept of a floating photocatalytic material for facile and effective water remediation with repeated usability.

Received 4th November 2023
Accepted 12th December 2023

DOI: 10.1039/d3ra07534f

rsc.li/rsc-advances

Introduction

Remediation of contaminated wastewater is one of the biggest environmental challenges.[1–3] In particular, the worldwide production of dye wastewater reaches 70 000 000 tons per year, and its purification is an urgent need.[4–6] As common strategies of waste water treatment, adsorption, filtration, chemical and/or biological oxidation are used, whereas those treatments have limitations such as short useful life, lack of performance and secondary pollution.[7,8] Recently, photocatalytic wastewater purification has been explored as an alternative to the adsorption-based method, with its efficient purification under sunlight and long-term usability with continuous photocatalytic activity.[9] In a photocatalytic system, electrons in the valence band were excited upon light illumination, generating holes in the valence band and the electrons move to the conduction band.[10] These excitons can react with H_2O and O_2 molecules in water, generating hydroxyl and superoxide radicals that can participate in degradation of an organic pollutant.[11] For an effective radical generation, it is crucial to maintain the separation between photo-excited electrons and holes, demoting the charge-hole recombination.[12] As an effective strategy of suppressing the electron–hole recombination, various heterojunction systems of semiconductor-based photocatalysts have been suggested.[13] Moreover, heterojunction photocatalysts promoted reactivity under visible light, with efficient electron–hole separation and efficient charge transferability. These features make them particularly well-suited for application in photocatalytic wastewater purification.[14] To design an effective heterojunction photocatalyst, appropriate semiconductors need to be selected.[15]

Metal–organic frameworks (MOFs) have been suggested as an attractive option for water purification by degrading the water-dissolved organic pollutants.[16,17] In recent studies, MOFs are favored in numerous fields due to their high surface area and structural tailorability.[18] In particular, high adsorption capacity of MOFs against the target molecules can promote the photocatalytic degradation at the surface.[19] Recently, silver halides (AgCl, AgBr, AgI) have been studied as effective photocatalysts with high photocatalytic activity in a wide range of wavelength including the visible light.[20,21] However, silver halides are vulnerable to photocorrosion induced by the photogenerated electrons in the conduction band, reducing silver ions to Ag^0.[22,23] The photocorrosion can lead to the decomposition of silver halide crystal structure under light irradiation,

[a]*Department of Fashion and Textiles, Seoul National University, Seoul 08826, Republic of Korea. E-mail: jkim256@snu.ac.kr*

[b]*Research Institute of Human Ecology, Seoul National University, Seoul 08826, Republic of Korea*

† Electronic supplementary information (ESI) available. See DOI: https://doi.org/10.1039/d3ra07534f

limiting repeated use of silver halides.[21] When silver halides form a heterojunction system with other photocatalysts, the enhanced charge transfer attributed to the heterojunction system prevents the accumulation of photogenerated electrons in the conduction band of silver halides, preventing the photocorrosion.[24] This mechanism allows the effective photocatalysis of silver halides in a heterojunction system.[25] Moreover, when silver halides are used as components of heterojunction photocatalysts, the reduced Ag nanoparticles can act as an electron transfer intermediate, conducing to a higher photocatalytic activity.[26]

The powdery form of photocatalyst, when used for purification of a wasted solution, has disadvantages as the light absorption becomes inefficient when the particles are sunk in the solution and the recovery of particles after use is inconvenient.[27] Those factors can hinder the practical application of powdery photocatalysts in water purification.[5] To overcome those drawbacks, efforts have been made to immobilize or synthesize the photocatalytic compounds on a substrate such as glass, fiber, and hydrogel in composite forms.[28–31] In fact, the penetration of sunlight is extremely restricted, even 90% of incident solar radiation is adsorbed by water when exceeds depth of 20 m.[32] In that case, a floating substrate loaded with catalysts can be an attractive means to maximize the light utilization.[33–35] The floating methods from earlier studies employed materials with low specific gravity, such as porous sponge, carbonized cellulose, cork, and perlite.[36–39] For the optimized photocatalytic performance, the floating photocatalyst should be designed to have sufficient contact with target pollutants, high loading capacity and high durability with strong bonding with photocatalysts.[5,36]

Herein, a durable floating photocatalytic composite in a woven construction is proposed. For an efficient photocatalytic remediation of water, polluted with Rhodamine B (RhB) dye, a heterojunction photocatalysts of UiO-66-NH_2 and AgI were immobilized on a cotton yarn substrate.[40,41] The cotton yarn treated with those photocatalysts was woven with the untreated polypropylene (PP) yarn with a low specific gravity to construct a floating woven fabric. UiO-66-NH_2, a zirconium-based MOF was employed in this study due to its applicability in the visible light range.[42] UiO-66-NH_2 was synthesized on cotton yarn *via in situ* solvothermal method. AgI, as an efficient photocatalyst under the visible light as well, was synthesized on the surface of UiO-66-NH_2 by the ion-exchange method, resulting in a heterojunction photocatalytic system. AgI is a preferred option of photocatalyst among the silver halides, due to its higher light sensitivity and stability compared to AgBr or AgCl. AgI also has a lower conduction band energy than other silver halides, leading to a higher redox potential.[43] RhB was used as a model contaminant, and the applicability of the suggested system was demonstrated with various experimental setups. The photodegradation mechanisms are investigated on the reactive oxygen species (ROS) that are responsible for the degradation process. The rate of RhB removal was analyzed for its kinetics of adsorption process and that of photocatalytic reaction, and informative discussion was made on the rate-determining step in different stirring conditions. This study intends to offer a facile yet effective photocatalytic system for water remediation, employing a floating woven construction.

Experimental section

Materials

Zirconium(IV) chloride ($ZrCl_4$) anhydrous (≥95%) was purchased from Sigma-Aldrich (USA). 2-Aminoterephthalic acid (99%) was purchased from Thermo Fisher Scientific Inc. (USA). Rhodamine B was purchased from Seoul Chemical Co. Ltd (Korea). Ammonium oxalate monohydrate (AO, 99.5%) was purchased from Junsei Chemical Co., Ltd (Japan). *N*,*N*-Dimethylformamide (DMF, 99.5%), ethanol (99.9%), hydrochloric acid (HCl, 35–37%), chloroacetic acid (99%), sodium hydroxide (NaOH, ≥ 95%), *p*-benzoquinone (*p*-BQ, 98%), isopropanol (IPA, 99.5%), potassium iodide (KI, 99.5%), and 0.1 M of silver nitrate solution ($AgNO_3$, 98–99%) were purchased from Daejung Chemicals (Korea). Cotton yarn (0.28 g m^{-1}) and polypropylene (PP) yarn (0.5 g m^{-1}) were used to weave fabrics.

Materials preparation of AgI/UiO@fabric

Cotton yarn was used after scouring with a detergent solution to remove any impurities. For the scouring solution, 0.24 g of NaOH, 1.2 g of H_2O_2, and 0.12 g of neutral detergent were dissolved in 120 mL of distilled water. A 1 g of cotton yarn was scoured in this solution at 90 °C for 15 min, then rinsed with distilled water. In order to make the seeding sites for growth of UiO-66-NH_2, 1 g of scoured cotton yarn was carboxymethylated by immersing in 100 mL of aq. solution with 9.5 g of chloroacetic acid and 15 g of NaOH. The yarn was treated for 72 h, then rinsed with distilled water several times. UiO-66-NH_2 was synthesized onto the carboxymethylated cotton yarn by the solvothermal method.[44] For the metal solution, 0.125 g of $ZrCl_4$ was dissolved in 5 mL of DMF and 1 mL of 37% HCl. A 90 cm (approximately 0.3 g) of cotton yarn was immersed into the metal solution for 10 min with stirring to induce interactions between Zr^{4+} ions and –COOH group of the carboxymethyl cotton. Then a linker solution with 0.135 g of 2-aminoterephthalic acid in 5 mL of DMF was added into the metal solution containing the cotton yarn. The mixed solution was stirred for 5 min, and kept in oven at 80 °C for 3 h. Finally, UiO-66-NH_2-grown cotton yarn (UiO@cotton) was washed sequentially with DMF, ethanol, and distilled water.

An ion-exchange method was used to synthesize AgI at the surface of UiO@cotton. First, a UiO-66-NH_2 cotton yarn was immersed into 35 mL of 0.3 mmol of aq. KI solution with stirring for 1 h to facilitate the ionic bonding between the zirconium ions of UiO-66-NH_2 and the iodine ions. Subsequently, 3 mL of 0.1 M $AgNO_3$ solution was added dropwise, keeping it 12 h for synthesis of AgI crystals on UiO@cotton. The produced AgI/UiO@cotton was washed with distilled water several times and stored in a thermo-hygrostat at 25 °C and 50% RH (Platinous J, ESPEC, Japan). The AgI@cotton was synthesized in the same way on carboxymethylated cotton skipping the process for UiO-66-NH_2 synthesis.

To fabricate a photocatalytic AgI/UiO@fabric that floats on water, 90 cm AgI/UiO@cotton yarn was woven with PP yarn in a plain weave construction of 4 PP warp × 6 cotton weft per cm^2. The AgI/UiO@fabric with 2.5 cm × 2 cm (containing 13 photocatalytic yarns and 10 PP yarns) was used as a test specimen, where it contained approximately 0.12 g of PP yarn, and 0.25 g of AgI/UiO@cotton yarn.

Characterization

The morphology of the fabric sample was analyzed by the field-emission scanning electron microscope (FE-SEM) and transmission electron microscope (TEM). The crystal structure of photocatalyst was analyzed by an X-ray diffractometer (XRD, SmartLab, Rigaku, Japan), and the chemical bonds of the Zr, N, Ag, I, and O elements were studied by an X-ray photoelectron spectrometer (XPS, AXIS SUPRA, Kratos, U.K.). To measure the light absorption of the fabric samples, UV-vis absorbance of each AgI@fabric, UiO@fabric, and AgI/UiO@fabric was analyzed by a UV-vis spectrophotometer (UV-2600, Shimadzu, Japan). The band gap energy (E_g) of each photocatalytic fabric was calculated from DRS data using the Kubelka–Munk equation (eqn (1)) with $n = 1$; where α is absorption coefficient; h is Planck constant, ν is light frequency, A is Tauc's constant, and E_g is absorption coefficient.[45]

$$\alpha h\nu = A(h\nu - E_g)^{n/2} \quad (1)$$

Photodegradation test

RhB was used as a model pollutant, and the photocatalytic degradation of aq. RhB solution (50 mL of 10 mg L^{-1} RhB) was tested. For the controlled test in the visible light, a xenon lamp was used under 150 W with UV cut-off filter (>400 nm, 100 mW cm^{-2}). Without a pre-adsorption step, a photocatalytic fabric (2.5 cm × 2 cm) was floated on a dye solution, with stirring at the bottom of the solution. Each photodegradation experiment was conducted for 2 h under a light source, and an aliquot of 0.6 mL of solution was extracted every 20 min to measure the RhB concentration. The concentration of RhB solution was measured by UV-vis absorbance spectroscopy (Synergy H1, BioTek, USA) at the wavelength of 553 nm.

An outdoor photodegradation test was conducted to simulate a practical application of water remediation under the actual daylight from 10:00 am to 17:00 pm. In this test, a 50 mL of RhB solution with a floating photocatalytic fabric was kept under the direct sunlight without any manipulation such as stirring.

Result and discussion

Characterization of photocatalytic fabric

The morphologies of carboxymethylated cotton, UiO@cotton, and AgI/UiO@cotton are presented in Fig. 1a–c. From Fig. 1b of UiO@cotton, UiO-66-NH_2 crystals in 50–100 nm were observed on the surface of carboxymethylated cotton. From the SEM and

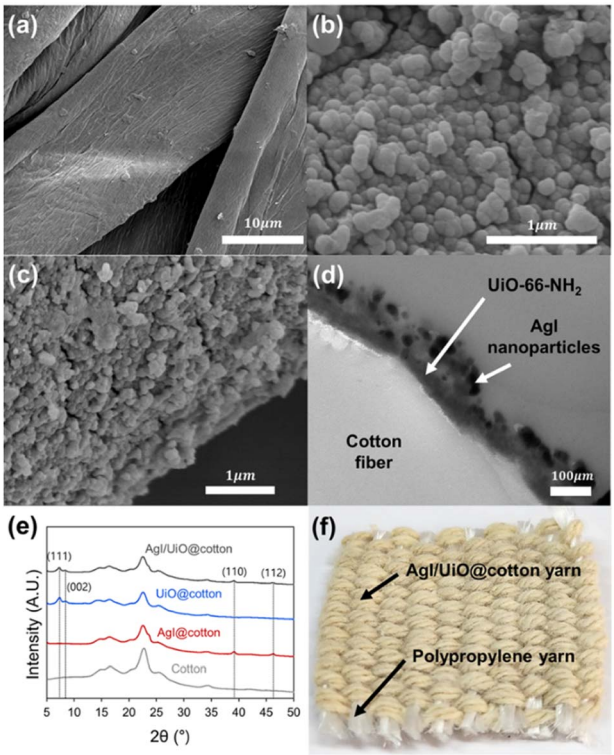

Fig. 1 SEM images of (a) carboxymethylated cotton, (b) UiO@cotton, and (c) AgI/UiO@cotton. (d) TEM image of AgI/UiO@cotton. (e) XRD data of cotton, AgI@cotton, UiO@cotton, and AgI/UiO@cotton. (f) Photograph of floating AgI/UiO@fabric in woven construction.

TEM images of AgI/UiO@cotton in Fig. 1c and d, AgI nanoparticles were grown on the surface of UiO-66-NH_2 crystals, giving a layered structure of AgI and UiO-66-NH_2 on cotton surface. The X-ray diffraction (XRD) analyses of prepared samples are shown in Fig. 1e. A carboxymethylated cotton produced broad diffraction peaks at 13–18° and 20–25°, corresponding to (110) and (200) planes of cellulose.[46] After the solvothermal synthesis of UiO-66-NH_2 on the carboxymethylated cotton fiber, UiO@cotton showed characteristic diffraction peaks at 7° and 8°, corresponding to (111) and (002) plane of UiO-66-NH_2.[47] Similarly, by direct synthesis of AgI nanocrystals on the carboxymethylated cotton fiber without synthesis of UiO-66-NH_2, AgI@cotton showed characteristic peaks at 39° and 46°, which are corresponding to (110) and (112) plane of AgI.[48] As for AgI/UiO@cotton, the aforementioned characteristic peaks of UiO-66-NH_2 and AgI crystals are observed clearly, indicating the existence of both AgI and UiO-66-NH_2 on the cotton yarn. The photograph of AgI/UiO@fabric in woven construction showed in Fig. 1f. FT-IR analysis was conducted on carboxymethylated cotton, UiO@cotton, and AgI/UiO@cotton (Fig. S1†). In all samples, a broad peak representing –OH group appeared at 3300 nm^{-1}, and a peak indicating C=O double bonds was observed at 1710 nm^{-1}.[49] Although most of the peaks were inundated by cotton substrate, the distinct peak of Zr–COO^- attributed to UiO-66-NH_2 was observed at 1573 cm^{-1} in both UiO@cotton and AgI/UiO@cotton.[50]

X-ray photoelectron spectroscopy (XPS) was applied to characterize the surface chemistry of photocatalysts for verification of (1) presence of UiO-66-NH_2 and AgI crystals, (2) chemical bonding as an evidence of heterojunction between UiO-66-NH_2 and AgI crystals. Fig. S2† shows the survey spectrum of photocatalysts and C, N, O, Ag, I and Zr elements. Regarding the Zr 3d spectrum (Fig. S3a and b†), two peaks at 182.5 eV and 184.8 eV were ascribed to Zr^{4+} $3d_{5/2}$ and $3d_{3/2}$, respectively, suggesting the formation of Zr–O bonds in the metal cluster of UiO-66-NH_2.[40] The high resolution N 1s spectrum shows three peaks attributed to –NH–, $-NH_2$, and $-NH_3^+$, which reveals the presence of UiO-66-NH_2 (Fig. S3c†).[47,51] However, in Fig. S3d,† the N 1s pattern has changed with growth of AgI crystals on UiO-66-NH_2. The characteristic peaks of $-NH_3^+$ (401.9 eV) disappeared while –NH– and $-NH_2$ peaks were still preserved, implying that $-NH_3^+$ was used as a growth site for AgI crystals. Also, successful synthesis of AgI on both AgI@cotton and AgI/UiO@cotton was confirmed from the spectra of $3d_{3/2}$ and $3d_{5/2}$ peaks of Ag and I elements (Fig. 2a–d).[40,52] It is noted that the offset of binding energy represents the change of surface charge density; for example, an increase in the binding energy suggests the reduced electron density.[40] In this analysis, it is speculated that the changes of electron density in hybrid materials result from the formation of heterojunction. Compared with AgI@cotton, the peaks of Ag $3d_{3/2}$, Ag $3d_{5/2}$, I $3d_{3/2}$, and I $3d_{5/2}$ in the AgI/UiO@cotton were blue-shifted to higher values, and it suggests the evidence of heterojunction in the system of AgI and UiO-66-NH_2.

Light absorbance of AgI@fabric, UiO@fabric, and AgI/UiO@fabric was analyzed by UV-vis diffuse reflectance spectroscopy (DRS), to observe the optical properties along the wavelength and estimate the band gap energy. As displayed in Fig. 2e, AgI/UiO@fabric presents stronger visible-light absorption intensities compared to AgI@fabric or UiO@fabric, demonstrating the enhanced absorption capability of visible light. The band gap energy (E_g) of each photocatalytic fabric was calculated in Fig. S4† from DRS data and using the Kubelka–Munk equation. UiO@fabric and AgI/UiO@fabric showed the same band gap energy of 2.75 eV while AgI@fabric showed slightly higher band gap energy of 2.78 eV. The band gap energies indicate that all of these materials can be activated under the visible light.

The steady-state photoluminescence spectroscopy (PL) was performed to observe the phenomena of electron–hole pair recombination in the heterojunction system. Upon the light irradiation, electrons were excited to a higher energy level, and the energy is released when the excited electrons return to a lower energy.[53] A lower intensity of the PL spectra is interpreted as the lower recombination tendency of electron–hole pairs, inducing the more efficient photocatalytic activity. Fig. 2f presents PL emission spectra of UiO@cotton and AgI/UiO@cotton excited at 400 nm. The UiO@cotton exhibited a strong emission in range of 450–470 nm, implying a higher recombination tendency of electron–hole pairs. The similar emission can be seen in the AgI/UiO@cotton with relatively weak PL intensity. This reduced PL intensity implies the recombination tendency is lowered by the efficient electron–hole separation between AgI and UiO-66-NH_2 heterostructure.

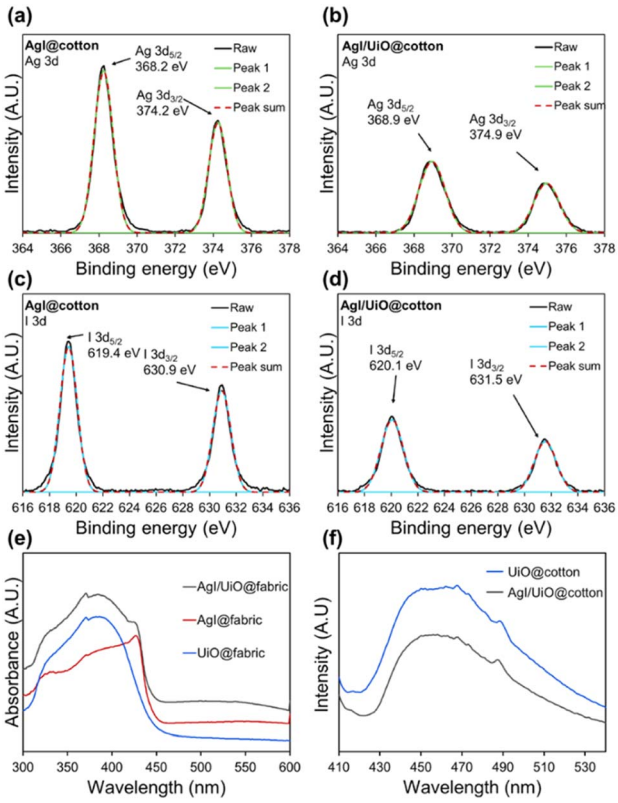

Fig. 2 High resolution XPS curves of (a) Ag 3d of AgI@cotton, (b) Ag 3d of AgI/UiO@cotton, (c) I 3d of AgI@cotton, and (d) I 3d of AgI/UiO@cotton. (e) UV-vis DRS of photocatalytic fabrics. (f) PL spectra of UiO@cotton and AgI/UiO@cotton.

RhB photodegradation test

The removal of RhB, attributed to simultaneous adsorption and photodegradation, was examined under visible light irradiation without pre-adsorption step. The observation of the combined effect is relevant as the adsorption would occur continuously as the photodegradation progresses.[54] Also, this test setup properly represents an actual water remediation process where both adsorption and photodegradation occur concurrently. To compare with the RhB removal efficiency by the adsorption

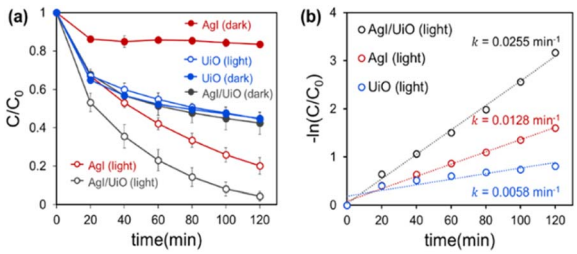

Fig. 3 (a) Rhodamine B removal (%) by the photocatalytic fabrics under 150 W xenon lamp. (b) First-order kinetics of Rhodamine B removal in photocatalytic reactions.

only, the test was additionally conducted in dark without activating photodegradation. In Fig. 3a, UiO@fabric removed 65% of RhB by adsorption (in dark) during 120 min, while AgI@fabric adsorbed only 17% of RhB. This higher adsorption of UiO@fabric results from the large surface area of UiO-66-NH_2 and the strong electrostatic interaction between cationic RhB and negatively charged UiO-66-NH_2.[55] The band gap of UiO@fabric was measured to be 2.75 eV from DRS analysis (Fig. S4†), indicating that the photodegradation would be activated under the visible light. However, the photodegradation of UiO-66-NH_2 under visible light was negligible, as is shown from Fig. 3a, where RhB removal of UiO@fabric was comparable between dark and light conditions. Even though the required band gap energy is sufficiently low to excite the electrons under the visible light, it appears that effective generation of ROS is inhibited due to the rapid recombination of excited electrons and holes.[56] As demonstrated in characterization section, the PL spectra of Fig. 2f supports the rapid recombination of UiO-66-NH_2 with higher PL intensity than that of AgI/UiO heterojunction photocatalyst.

In Fig. 3a, AgI treated fabric showed little adsorption capacity from the 'dark' test, and the removal efficiencies of AgI/UiO@fabric (dark) and UiO@fabric (dark and light) were comparable. However, under the visible light, RhB removal efficiency of AgI@fabric reached up to ~80% during 120 min while that in dark was only 17%; this verifies that photocatalytic effectiveness of AgI in the visible light range. For AgI/UiO@fabric, AgI crystals were synthesized on the surface of UiO@fabric, and it showed 98% of removal efficiency under visible light. In dark, AgI/UiO@fabric exhibited similar adsorption capacity as the UiO@fabric. The enhanced RhB removal efficiency of AgI/UiO@fabric under light, compared to UiO@fabric, is attributed to the combined effect of adsorption and photodegradation of AgI/UiO heterojunction catalysts.[57]

The rate of RhB removal was evaluated by the first-order rate constant in Fig. 3b, where it demonstrates the first-order rate constant of AgI/UiO@fabric under light (0.0255 min^{-1}) was approximately two times higher than that of AgI@fabric (0.0128 min^{-1}), and four times higher than that of UiO@fabric (0.0058 min^{-1}). As the RhB removal of UiO@fabric depends solely on the adsorption, the rate was lowest among the tested samples. On the other hand, even AgI@fabric showed photocatalytic activity, removal rate was still lower than AgI/UiO@fabric. AgI/UiO@fabric displayed the highest removal rate due to the combined effect of adsorption (by UiO-66-NH_2) and photodegradation that was enhanced by heterostructure of AgI and UiO-66-NH_2.

Photodegradation mechanism of AgI/UiO-66-NH_2 heterojunction system

The reactive chemical species contributing to the photodegradation was investigated by testing with the scavenging chemicals of different reactive species for AgI/UiO@fabric. A 1 mL of each 0.05 M *p*-benzoquinone (*p*-BQ), isopropanol (IPA), and ammonium oxalate (AO) solution was used to capture superoxide radical ($^{\bullet}O_2^-$), hydroxyl radical ($^{\bullet}OH^-$), and hole (h^+), respectively. The efficiency of photodegradation was calculated by eqn (2), where C_{dark} is the removal efficiency (%) in dark, presumably attributed by adsorption; C_{light} is the removal efficiency (%) under light attributed by both adsorption and photodegradation; and $C_{scavenger}$ is the removal efficiency (%) with scavenging chemicals under light, which cancels out the photodegradation effect of corresponding reactive species. In Fig. 4a, the removal efficiency of AgI/UiO@fabric tested in dark was attributed to the adsorption by UiO-66-NH_2. Comparing with the removal efficiency without the scavenger (Fig. 4b), the photodegradation was considerably suppressed in presence of *p*-BQ, which indicates that superoxide radicals played a major role in photodegradation process. The effects of other reactive species were rather marginal.

$$\text{Photodegradation attributed to the respective reactive species (\%)} = \frac{C_{dark} - C_{scavenger}}{C_{dark} - C_{light}} \quad (2)$$

Understanding that superoxide radical ($^{\bullet}O_2^-$) is the main contributor to the photodegradation, further investigation on the reaction mechanism of AgI/UiO@fabric for RhB degradation was conducted. From the UV-vis spectrum in Fig. 5a, the reaction without scavenger (under light) showed a huge decline of peak at 553 nm, accompanying blue shifting of the major peak. This blue shifting of the peak is attributed to de-ethylation of RhB (maximum absorbance at 553 nm) to Rhodamine (Rh) that displays the maximum absorbance at 498 nm.[58] As this transformation is also featured in AgI@fabric (Fig. S5†), the de-ethylation of RhB appears to be triggered by AgI catalyst. Notably, when *p*-BQ was added to capture $^{\bullet}O_2^-$ radicals (for AgI/UiO@fabric), the blue shifting was not observed while the peak at 553 nm showed obvious decline dominated by the adsorption (Fig. 5b). The interruption of blue shifting by *p*-BQ implies that $^{\bullet}O_2^-$ are the main contributor to de-ethylation of RhB to Rh. The other scavenging species showed no evidence of de-ethylation or blue-shifting.

When IPA scavenger was added, the spectrum showed no change from the one without scavengers, implying $^{\bullet}OH^-$ was not a contributing reactive species (Fig. 5c). When AO was

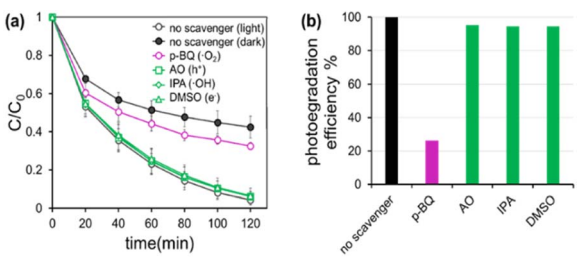

Fig. 4 Reactive chemical species contributing to photodegradation, investigated by the scavenging chemicals corresponding to reactive species. (a) RhB removal efficiency for AgI/UiO@fabric with and without scavenging chemicals, (b) Photodegradation effect of AgI/UiO@fabric calculated by eqn (2), with and without scavengers.

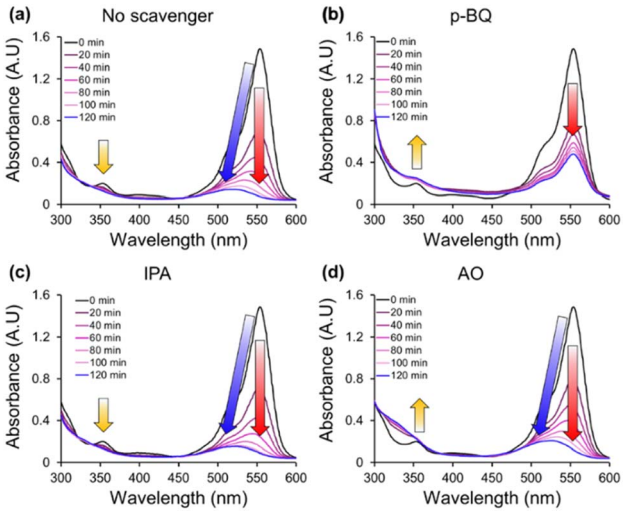

Fig. 5 UV-vis absorbance spectra of Rhodamine B with AgI/UiO@fabric under visible light with (a) no scavenger, (b) *p*-benzoquinone (*p*-BQ), (c) isopropanol (IPA), and (d) ammonium oxalate (AO).

added as the scavenger of h^+, peak at 553 nm declined and blue shifting occurred similarly with the reactions without scavengers (Fig. 5d). However, the tendency of peak evolvement in UV region (around 350 nm) was different for AgI/UiO@fabric with and without AO scavenger. Since the decrease of absorbance in UV region indicates the dissociation of aromatic ring in RhB, it is inferred that h^+ participated in decomposition of aromatic ring.[59]

Facile application of AgI/UiO@fabric under sunlight

Photocatalytic performance under the natural sunlight was tested to validate the applicability of the developed photocatalytic fabric for facile water remediation. AgI/UiO@fabric was thrown onto the RhB solution without any manipulative operation such as stirring. The photograph of experimental setup in Fig. 6a demonstrates that the density of the woven fabric is well adjusted to float on surface, and the floating status lasted even after 4 weeks. As a result, the treated photocatalysts not only maximized the sunlight absorption but also efficiently interacted with the dissolved RhB.[35] To note, the floating fabric was optimized by adjusting the fabric density by the blend ratio of PP yarn. Despite that removal performance was different for the testing day, all tested AgI/UiO@fabrics displayed over 55% of RhB removal efficiency under sunlight (7 h) whereas the removal in dark (7 h) was less than 25% (Fig. 6b).

The advantage of floating characteristic on the photocatalytic efficiency was verified by the comparative testing with fabrics in different densities (Fig. 6c). In this experiment, a 100 mL of 10 mg L^{-1} RhB solution was contained in a narrow cylindrical reactor, and the side of the reactor was screened to block the light from sides. Only the light through the top was available to induce the photodegradation. The difference in depth between the floating and submerged samples was approximately 15 cm. In Fig. 6c, a floating AgI/UiO@fabric showed removal efficiency of 33%, while the submerged AgI/UiO@fabric removed only 12% over 8 h. This result indicates that the floating system was much more effective in utilizing the light for photocatalytic reactions. The test demonstrates the practical applicability of this proof-of-concept fabric as a floating purification system without intricate manipulative operations.

Kinetics of RhB removal by AgI/UiO@fabric

As the most photodegradation mostly occurs on the surface of the photocatalyst rather than in the bulk solution, an effective adsorption of pollutant is an important factor affecting the photodegradation performance.[57] To analyze the effect of RhB-catalyst interaction (or solution circulation) on the photodegradation, stirring conditions were varied (Fig. 7). In this analysis, the overall RhB removal efficiency was analyzed for the removal attributed to adsorption ($C_0 - C_{dark}$) tested in dark, and the removal attributed to photodegradation ($C_{dark} - C_{light}$) tested under the visible light; where C_0 is RhB concentration at time 0, C_{dark}, and C_{light} are RhB concentration at time t under dark and light, respectively. The removal attributed to the photodegradation was estimated by subtracting the adsorption effect in dark from the overall removal under light irradiation.

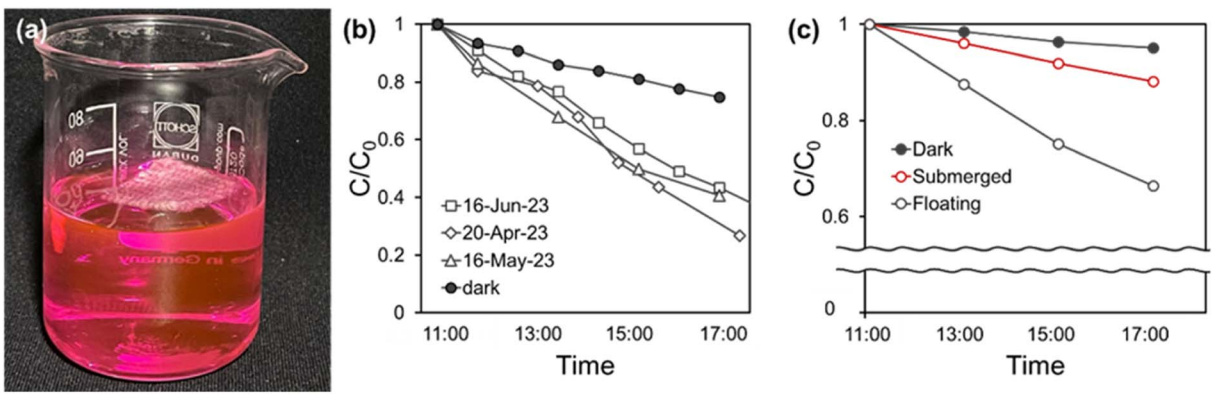

Fig. 6 Practical application of the floating photocatalytic AgI/UiO@fabric tested under natural sunlight. (a) Photograph of floating AgI/UiO@fabric in RhB solution. (b) RhB removal efficiency under sunlight in different days. (c) Comparative test of floating and submerged fabrics for RhB removal efficiency.

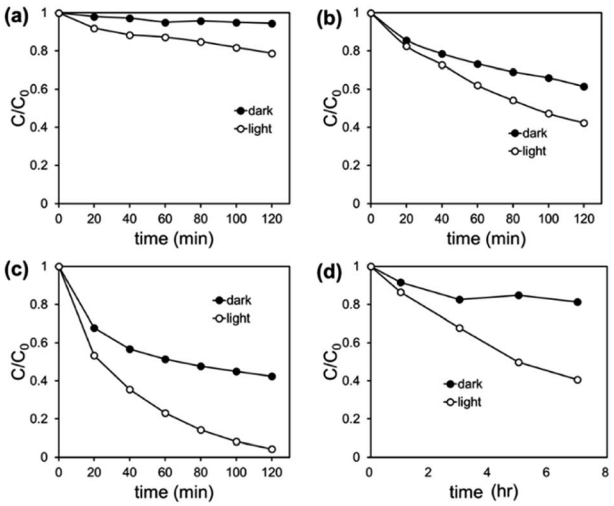

Fig. 7 Rhodamine B removal (%) by AgI/UiO@fabric under 150 W xenon lamp (a) without stirring (0 rpm), (b) with stirring at 200 rpm, and (c) stirring at 700 rpm. (d) Rhodamine B removal (%) by AgI/UiO@fabric under sunlight.

Each adsorption rate and photodegradation rate was estimated by the first-order kinetics model following eqn (3) and (4), respectively; and k is the first-order rate constant.

$$-\ln\left(\frac{C_{\text{dark}}}{C_0}\right) = kt \quad (3)$$

$$-\ln\left(\frac{C_{\text{dark}} - C_{\text{light}}}{C_0}\right) = kt \quad (4)$$

Table 1 shows the first-order rate constant under varied stirring conditions. When RhB solution was treated with stirring at 700 rpm, the adsorption was relatively faster (k_{ad}, 0.0064 min^{-1}) than the photodegradation (k_{pd}, 0.0040 min^{-1}). This result implies that photodegradation was the rate-determining step in the whole removal process, determining the overall removal rate. In a moderate stirring condition at 200 rpm, both adsorption and photodegradation rates were reduced, and the photodegradation rate (k_{pd}, 0.0019 min^{-1}) was still lower than the adsorption rate (k_{ad}, 0.0038 min^{-1}). However, without stirring (0 rpm) where only the spontaneous adsorption occurred by diffusion of RhB, the reaction rates were reversed, with k_{pd} (0.0012 min^{-1}) being greater than k_{ad} (0.0004 min^{-1}). This indicates that, without stirring, adsorption was the rate-determining step of the whole removal process, determining the overall removal rate. This reversed reaction rates of adsorption and photodegradation under no stirring indicate that the amount of adsorbed RhB was fall short of consistently generated reactive oxygen species from photocatalysts.[57,60] The removal of RhB under the natural sunlight, tested without stirring, showed the same tendency of lower adsorption (k_{ad}, 0.0004 min^{-1}) than photodegradation (k_{pd}, 0.0013 min^{-1}). This result implicates that adsorption may determine the overall removal rate in still water, and facilitated adsorption of pollutants to the surface of photocatalyst would eventually accelerate the overall photodegradation process in water purification system.

Recycle test

For practical applications, adapting washing processes for photocatalytic composite can be cumbersome; and the recyclability and the stability of the photocatalytic system are important factors to be considered.[61] To test the long-term applicability of the developed photocatalytic fabric, recycle tests were conducted without applying any washing or desorption process (Fig. 8a). From the second removal tests, the removal rates (or slope) at the earlier stage were lower than that from the first cycle test, presumably because adsorption sites were mostly occupied in the first cycle. While the adsorption could occur dominantly in the early stage of the first cycle, the removal efficiency in the repetitive cycles was mostly preserved due to the consistent photodegradation performance. XRD

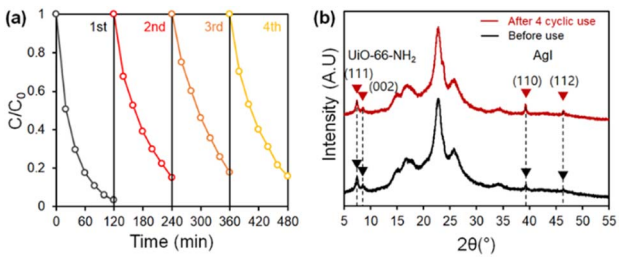

Fig. 8 (a) Recycling tests of AgI/UiO@fabric under the visible light. (b) XRD patterns of AgI/UiO@fabric before and after cyclic tests.

Table 1 First-order rate constants of adsorption and photodegradation under various adsorption conditions

1st order kinetic constant	700 rpm	200 rpm	0 rpm	0 rpm
k_{ad}	Under dark 0.0064 min^{-1}	0.0038 min^{-1}	0.0004 min^{-1}	0.0004 min^{-1}
1st order kinetic constant	700 rpm	200 rpm	0 rpm	0 rpm
k_{pd}	Under 150 W xenon lamp 0.0040 min^{-1}	0.0019 min^{-1}	0.0012 min^{-1}	Under sunlight 0.0013 min^{-1}

analysis before and after the cyclic tests (Fig. 8b) revealed that the crystal structure of AgI/UiO-66-NH_2 on the fabric remained unchanged after 4 times of cyclic uses. The result shows the long-term applicability of the developed AgI/UiO@fabric for the facile water purification even without washing procedure, maintaining structural integrity and catalytic stability. To examine the leaking of adhered photocatalysts on the fabric, the photocatalytic reaction was simulated by immersing the fabric in distilled water and stirring for 2 h with irradiation. After 2 h stirring, the reacted water was collected to observe UV-vis absorbance using distilled water as a baseline; any absorbance change from distilled water could come from the detached catalytic particles. In Fig. S6,† the water solution from AgI@fabric showed higher absorbance at 420 nm, corresponding to Ag^+ ions, than that of AgI/UiO@fabric.[62] This demonstrates the higher amount of Ag^+ and particle detachment from AgI@fabric; on the other hand, AgI/UiO heterojunction photocatalyst showed stronger adhesion on the fabric.

The results demonstrate that the proof-of-concept photocatalytic fabric well performs under the visible light, with efficient generation of reactive oxygen species. The floating fabric was advantageous in maximized utilization of light absorption and efficient adsorption of contaminant. The kinetic study suggests that the facilitated adsorption can expedite the overall photodegradation process. Further study on the kinetics of adsorption, desorption and catalytic processes is recommended to clarify the intricate interactions of those processes.

Conclusions

Floating photocatalytic fabric was developed in a woven construction for wastewater treatment. For an efficient photodegradation, a heterojunction system was created by synthesizing UiO-66-NH_2 and AgI nanocrystals sequentially on the carboxymethylated cotton yarn *via* solvothermal and ion-exchange methods, respectively. It showed a layered structure of UiO-66-NH_2 covered by AgI nanocrystals on the surface of cotton fiber. Through the heterojunction system, the recombination of excitons was suppressed, leading to an effective photodegradation of Rhodamine B. The photocatalytic cotton yarn was woven with polypropylene yarn, adjusting the fabric density to float on water surface. Compared to the individual treatment of UiO@fabric (65% RhB removal) or AgI@fabric (80% RhB removal), the heterojunction system of AgI/UiO@fabric showed much improved RhB removal efficiency (98%), due to the combined effect of adsorption and enhanced photodegradation performance resulting from the effective separation of electrons and holes. Superoxide radicals and holes contributed to the photodegradation of RhB by causing de-ethylation and aromatic ring decomposition, respectively. The practical applicability of floating AgI/UiO@fabric to wastewater treatment was tested *via* experiments under natural sunlight, comparing with submerged sample. Kinetic analysis on RhB removal by AgI/UiO@fabric implies that the facilitated adsorption, or effective supply of contaminants to photocatalyst, would eventually expedite the overall removal process in water purification. The recycle test and analysis demonstrated the possible long-term applicability of the developed AgI/UiO@fabric with structural integrity and catalytic stability. This study offers a facile and effective strategy of water remediation with lasting performance and repeated use, and provides an informative discussion on the rate-determining factors in varied adsorption conditions.

Author contributions

Jaeseon Yoo: conceptualization, investigation, conceived the idea, designed the experiments and wrote the original draft. Jinwook Lee: designed the experiments, data curation and analysis. Jooyoun Kim: funding acquisition, project administration, supervision and writing review & editing.

Conflicts of interest

There are no conflicts to declare.

Acknowledgements

This work was supported by the National Research Foundation of Korea (NRF) grant funded by the Korea government (MSIT) (No. 2022R1A2C2003072).

References

1 S. T. Khan and A. Malik, *J. Hazard. Mater.*, 2019, **363**, 295–308.
2 W. S. Chai, J. Y. Cheun, P. S. Kumar, M. Mubashir, Z. Majeed, F. Banat, S.-H. Ho and P. L. Show, *J. Cleaner Prod.*, 2021, **296**, 126589.
3 R. Mia, M. Selim, A. Shamim, M. Chowdhury, S. Sultana, M. Armin, M. Hossain, R. Akter, S. Dey and H. Naznin, *J. Text. Eng. Fash. Technol.*, 2019, **5**, 220–226.
4 H. Anwer, A. Mahmood, J. Lee, K.-H. Kim, J.-W. Park and A. C. K. Yip, *Nano Res.*, 2019, **12**, 955–972.
5 R. Al-Tohamy, S. S. Ali, F. Li, K. M. Okasha, Y. A.-G. Mahmoud, T. Elsamahy, H. Jiao, Y. Fu and J. Sun, *Ecotoxicol. Environ. Saf.*, 2022, **231**, 113160.
6 F. D. Guerra, M. F. Attia, D. C. Whitehead and F. Alexis, *Molecules*, 2018, **23**, 1760.
7 S. Bolisetty, M. Peydayesh and R. Mezzenga, *Chem. Soc. Rev.*, 2019, **48**, 463–487.
8 M. Al-Mamun, S. Kader, M. Islam and M. Khan, *J. Environ. Chem. Eng.*, 2019, **7**, 103248.
9 S. Kumar, W. Ahlawat, G. Bhanjana, S. Heydarifard, M. M. Nazhad and N. Dilbaghi, *J. Nanosci. Nanotechnol.*, 2014, **14**, 1838–1858.
10 Y. Gao, J. Wu, J. Wang, Y. Fan, S. Zhang and W. Dai, *ACS Appl. Mater. Interfaces*, 2020, **12**, 11036–11044.
11 D. Chen, Y. Cheng, N. Zhou, P. Chen, Y. Wang, K. Li, S. Huo, P. Cheng, P. Peng and R. Zhang, *J. Cleaner Prod.*, 2020, **268**, 121725.
12 C. Bie, H. Yu, B. Cheng, W. Ho, J. Fan and J. Yu, *Adv. Mater.*, 2021, **33**, 2003521.
13 Y.-J. Lai and D.-J. Lee, *Chemosphere*, 2021, **282**, 131059.
14 M. H. Abdurahman, A. Z. Abdullah and N. F. Shoparwe, *Chem. Eng. J.*, 2021, **413**, 127412.

15 L. Xie, T. Du, J. Wang, Y. Ma, Y. Ni, Z. Liu, L. Zhang, C. Yang and J. Wang, *Chem. Eng. J.*, 2021, **426**, 130617.
16 M. Jafarzadeh, *ACS Appl. Mater. Interfaces*, 2022, **14**, 24993–25024.
17 Y. Liu, Z. Liu, D. Huang, M. Cheng, G. Zeng, C. Lai, C. Zhang, C. Zhou, W. Wang, D. Jiang, H. Wang and B. Shao, *Coord. Chem. Rev.*, 2019, **388**, 63–78.
18 Q. Wang and D. Astruc, *Chem. Rev.*, 2020, **120**, 1438–1511.
19 X. Chen, X. Liu, L. Zhu, X. Tao and X. Wang, *Chemosphere*, 2022, **291**, 133032.
20 X.-J. Wen, C.-H. Shen, Z.-H. Fei, D. Fang, Z.-T. Liu, J.-T. Dai and C.-G. Niu, *Chem. Eng. J.*, 2020, **383**, 123083.
21 K. Huang, C. Li, Y. Zheng, L. Wang, W. Wang and X. Meng, *Sep. Purif. Technol.*, 2022, **283**, 120194.
22 B. Li, Z. Guo, Y. Feng and M. Meng, *J. Mater. Chem. A*, 2021, **9**, 16510–16521.
23 W. Li, F. Wang, X.-S. Chu, Y.-Y. Dang, X.-Y. Liu, T. Ma, J.-Y. Li and C.-Y. Wang, *Chem. Eng. J.*, 2022, **435**, 132441.
24 J. Li, B. Liu, X. Han, B. Liu, J. Jiang, S. Liu, J. Zhang and H. Shi, *Sep. Purif. Technol.*, 2021, **261**, 118306.
25 B. Weng, M.-Y. Qi, C. Han, Z.-R. Tang and Y.-J. Xu, *ACS Catal.*, 2019, **9**, 4642–4687.
26 X.-J. Wen, L. Qian, X.-X. Lv, J. Sun, J. Guo, Z.-H. Fei and C.-G. Niu, *J. Hazard. Mater.*, 2020, **385**, 121508.
27 H. S. Zakria, M. H. D. Othman, R. Kamaludin, S. H. S. A. Kadir, T. A. Kurniawan and A. Jilani, *RSC Adv.*, 2021, **11**, 6985–7014.
28 G. Singh, M. Sharma and R. Vaish, *Chem. Eng. J.*, 2021, **407**, 126971.
29 M. Qian, F. Yang, N. Li, J. Gao, X. Chen, T. Xu, Z. Zhu, W. Lu and W. Chen, *Chem. Eng. J.*, 2021, **414**, 128845.
30 Q. Guo, H. Sun, L. Zhang and D. Li, *Compos. Commun.*, 2021, **27**, 100846.
31 M. Zhang, W. Jiang, D. Liu, J. Wang, Y. Liu, Y. Zhu and Y. Zhu, *Appl. Catal., B*, 2016, **183**, 263–268.
32 T. A. Cooper, S. H. Zandavi, G. W. Ni, Y. Tsurimaki, Y. Huang, S. V. Boriskina and G. Chen, *Nat. Commun.*, 2018, **9**, 5086.
33 A. M. Nasir, J. Jaafar, F. Aziz, N. Yusof, W. N. W. Salleh, A. F. Ismail and M. Aziz, *J. Water Process Eng.*, 2020, **36**, 101300.
34 A. Rana, A. Sudhaik, P. Raizada, V.-H. Nguyen, C. Xia, A. A. Parwaz Khan, S. Thakur, P. Nguyen-Tri, C. C. Nguyen, S. Y. Kim, Q. V. Le and P. Singh, *Chemosphere*, 2022, **297**, 134229.
35 Z. Xing, J. Zhang, J. Cui, J. Yin, T. Zhao, J. Kuang, Z. Xiu, N. Wan and W. Zhou, *Appl. Catal., B*, 2018, **225**, 452–467.
36 J. Tang, J. Wang, L. Tang, C. Feng, X. Zhu, Y. Yi, H. Feng, J. Yu and X. Ren, *Chem. Eng. J.*, 2022, **430**, 132669.
37 Y. Chen, Y. Shi, H. Kou, D. Liu, Y. Huang, Z. Chen and B. Zhang, *ACS Sustainable Chem. Eng.*, 2019, **7**, 2911–2915.
38 M. Sboui, M. F. Nsib, A. Rayes, M. Swaminathan and A. Houas, *J. Environ. Sci.*, 2017, **60**, 3–13.
39 L. Noureen, Z. Xie, Y. Gao, M. Li, M. Hussain, K. Wang, L. Zhang and J. Zhu, *ACS Appl. Mater. Interfaces*, 2020, **12**, 6343–6350.
40 Y. Pan, X. Yuan, L. Jiang, H. Wang, H. Yu and J. Zhang, *Chem. Eng. J.*, 2020, **384**, 123310.
41 J. Liu, R. Li, Y. Hu, T. Li, Z. Jia, Y. Wang, Y. Wang, X. Zhang and C. Fan, *Appl. Catal., B*, 2017, **202**, 64–71.
42 G. Wang, C.-T. He, R. Huang, J. Mao, D. Wang and Y. Li, *J. Am. Chem. Soc.*, 2020, **142**, 19339–19345.
43 Z. Chen, W. Wang, Z. Zhang and X. Fang, *J. Phys. Chem. C*, 2013, **117**, 19346–19352.
44 H. N. Rubin, B. H. Neufeld and M. M. Reynolds, *ACS Appl. Mater. Interfaces*, 2018, **10**, 15189–15199.
45 P. Makuła, M. Pacia and W. Macyk, *J. Phys. Chem. Lett.*, 2018, **9**, 6814–6817.
46 S. Andra, S. K. Balu, J. Jeevanandam, M. Muthalagu and M. K. Danquah, *Cellulose*, 2021, **28**, 5895–5910.
47 X. Fang, S. Wu, Y. Wu, W. Yang, Y. Li, J. He, P. Hong, M. Nie, C. Xie, Z. Wu, K. Zhang, L. Kong and J. Liu, *Appl. Surf. Sci.*, 2020, **518**, 146226.
48 Q. W. Cao, Y. F. Zheng, H. Y. Yin and X. C. Song, *J. Mater. Sci.*, 2016, **51**, 4559–4565.
49 H. K. Nguyen, W. Sakai and C. Nguyen, *Materials*, 2020, **13**, 54.
50 T. Hashem, A. H. Ibrahim, C. Wöll and M. H. Alkordi, *ACS Appl. Nano Mater.*, 2019, **2**, 5804–5808.
51 X. Zou, S. Lou, C. Yang, N. Liu, X. Wang, L. Shi and X. Meng, *Catal. Lett.*, 2021, **151**, 487–496.
52 I. Ahmad, M. Muneer, A. S. Khder and S. A. Ahmed, *ACS Omega*, 2023, **8**, 22708–22720.
53 T. Kirchartz, J. A. Márquez, M. Stolterfoht and T. Unold, *Adv. Energy Mater.*, 2020, **10**, 1904134.
54 Y. Yu, D. Chen, W. Xu, J. Fang, J. Sun, Z. Liu, Y. Chen, Y. Liang and Z. Fang, *J. Hazard. Mater.*, 2021, **416**, 126183.
55 Z. U. Zango, K. Jumbri, N. S. Sambudi, H. H. Abu Bakar, Z. N. Garba, H. A. Isiyaka and B. Saad, *Polyhedron*, 2021, **210**, 115515.
56 Y. Tan, Y. Zhou, Y. Deng, H. Tang, H. Zou, Y. Xu and J. Li, *Colloids Surf., A*, 2021, **622**, 126699.
57 Y. Luo, X. Wei, B. Gao, W. Zou, Y. Zheng, Y. Yang, Y. Zhang, Q. Tong and L. Dong, *Chem. Eng. J.*, 2019, **375**, 122019.
58 Y. I. Choi, Y.-I. Kim, D. W. Cho, J.-S. Kang, K. Leung and Y. Sohn, *RSC Adv.*, 2015, **5**, 79624–79634.
59 X. Li and J. Ye, *J. Phys. Chem. C*, 2007, **111**, 13109–13116.
60 Y. Zhang, W. Cao, B. Zhu, J. Cai, X. Li, J. Liu, Z. Chen, M. Li and L. Zhang, *J. Colloid Interface Sci.*, 2022, **611**, 706–717.
61 W. Cao, Y. Zhang, Z. Shi, T. Liu, X. Song, L. Zhang, P. Keung Wong and Z. Chen, *Chem. Eng. J.*, 2021, **417**, 128112.
62 H. Liu, L. Yang, H. Ma, Z. Qi and J. Liu, *Chem. Commun.*, 2011, **47**, 9360–9362.